A Journal of the Gesellschaft Deutscher Chemiker

Angewandte International Edition GDCh Chemie

www.angewandte.org

Accepted Article

Title: Hypoxia-instructed pro-protein therapy assisted with self-catalyzed nanozymogen

Authors: Xudong Li, Yuansong Wei, Yuchen Wu, and Lichen Yin

To be cited as: *Angew. Chem. Int. Ed.* 10.1002/anie.202004008

Link to VoR: https://doi.org/10.1002/anie.202004008

WILEY-VCH

Hypoxia-instructed pro-protein therapy assisted with self-catalyzed nanozymogen

*Xudong Li[#],Yuansong Wei[#], Yuchen Wu, and Lichen Yin**

X. Li, Y. Wei, Y. Wu, Prof. Dr. L. Yin
Institute of Functional Nano & Soft Materials (FUNSOM),
Jiangsu Key Laboratory for Carbon-Based Functional Materials and Devices,
Collaborative Innovation Center of Suzhou Nano Science and Technology,
Soochow University,
Suzhou 215123, China
E-mail: lcyin@suda.edu.cn

X. Li and Y. Wei contributed equally.

Keywords

pro-protein engineering; intracellular protein delivery; hypoxia responsiveness; self-catalysis; starvation therapy

Abstract

The success of intracellular protein therapy demands potent intracellular delivery efficiency and selective protein activity in diseased cells. To fulfil these requirements, a cascaded nanozymogen incorporating hypoxia-instructed pro-protein engineering and hypoxia-strengthened intracellular protein delivery was developed. RPAB, a pro-protein of RNase A reversibly caged with hypoxia-cleavable azobenzene yet deprived of the enzymatic activity, was designed and co-delivered with glucose oxidase (GOx) using hypoxia-dissociable nanocomplexes (NCs) consisting of azobenzene-cross-linked oligoethylenimine (AOEI) and hyaluronic acid (HA). Upon NCs-mediated tumor targeting, cancer cell internalization, and endolysosomal escape, GOx catalyzed intracellular glucose decomposition and aggravated tumoral hypoxia, which drove the recovery of RPAB back to

10.1002/anie.202004008

the hydrolytically active RNase and concurrently expedited the degradation of AOEI to release more protein cargoes. Thus, the catalytic reaction of the nanozymogen was self-accelerated and self-cycled, ultimately leading to cooperative anti-cancer efficacies between GOx-mediated starvation therapy and RNase-mediated pro-apoptotic therapy. This study represents the first example of hypoxia-instructed pro-protein engineering, which expands the available chemical tools for the conditional control over protein functions. The self-catalyzed nanozymogen design also provides an effective strategy to mediate intracellular protein delivery and highly sensitive and selective intracellular pro-protein activation.

Protein therapeutics hold great potentials in the treatment of human diseases, mainly due to their higher specificity and less side effects over small-molecule drugs.[1] To date, clinically applied protein drugs are largely limited to those functioning extracellularly.[2] Although advancement in molecular biology has suggested that proteins targeting the intracellular machinery could be even more potent toward disease treatment,[3] protein therapeutics that exert bioactivity in the cytosol have achieved limited success,[4] because of the lack of efficient intracellular delivery vehicles that can transport the protein cargo to the diseased tissues, mediate trans-membrane delivery into target cells, avoid endolysosomal entrapment, and release the biologically active protein in the cytosol.[5] In the past years, various systems have been developed to enable intracellular protein delivery with exciting successes, as exemplified by dendrimer,[6] polymeric micells, [7] polymerized capsules,[8] cationic liposomes,[9] nanogels,[10] inorganic nanoparticles,[11] and etc.[12] However, effective vehicles that can harmonize all the above-mentioned delivery processes to mediate protein therapy *in vivo* are still of great demand.[13]

Another critical issue related to intracellular protein therapy is how to realize selective pharmacological activity in target cells, thus minimizing non-specific adverse effects to normal cells.[14] While the use of stimuli-responsive carriers can enable selective protein release in target cells, the inevitable pre-leakage or non-specific protein release would increase the risk of side toxicity.[15] Recently, the strategy of reversible caging of proteins with trigger-cleavable motifs has been explored to enable spatiotemporal control of protein function in response to chemical, biological, or physical signals, such as acid,[16] reactive oxygen species (ROS),[17] enzyme,[18] or light.[19] However, the potential of these protein

prodrugs in mediating selective protein therapy may still remain doubtful, mainly because of the insufficient sensitivity to exogeneous/endogenous triggers or the low specificity to discriminate between diseased and normal cells.[20] It is thus highly imperative to design caged protein prodrugs that are capable of highly efficient and selective de-caging in diseased cells, thus achieving maximized therapeutic efficacy and minimized systemic toxicity.

To fulfill the demands for the intracellular pro-protein therapy toward cancer treatment, we herein designed a hypoxia-activatable pro-protein, assisted with the construction of self-catalyzed cascaded nanozymogen to realize hypoxia-strengthened intracellular pro-protein delivery as well as sensitive and selective control over the hypoxia-instructed pro-protein activation in cancer cells. While various protein prodrugs capable of trigger-responsive activation have been reported,[16-19] hypoxia-instructed pro-protein engineering is still lacking, which makes it the first example of hypoxia-responsive protein prodrug. Particularly, RNase A was reversibly caged with hypoxia-cleavable azobenzene domains on its lysine residues, generating the pro-protein (RPAB) deprived of the enzymatic activity along with elevated net anionic charge density (Scheme 1). Thus, RPAB was deprived of the non-specific toxicity to normal cells. The azobenzene group could be reduced under hypoxic condition by the various reductases that are over-expressed and mainly localized inside tumor cells, thus restoring the hydrolytic activity of RNase intracellularly upon hypoxia-triggered uncaging of the azobenzene protection group. While the tumoral microenvironment is often hypoxic due to fast metabolism and proliferation of cancer cells, the hypoxia level in many solid tumors is heterogeneous and insufficient, which hurdles the effective re-activation of RPAB. As such, RBAP was co-delivered with glucose oxidase

(GOx), an enzyme that catalyzes the decomposition of glucose accompanied with concurrent exhaustion of O_2 and generation of H_2O_2.[21] Thus, GOx served to aggravate tumoral hypoxia and accordingly drive the recovery of RPAB back to RNase. To enable the targeted accumulation of protein drugs into tumor tissues and trans-membrane internalization into cancer cells, a cationic, hypoxia-degradable polymer based on azobenzene-cross-linked oligoethylenimine (AOEI) was further designed, which was allowed to form the nanozymogen upon electrostatic complexation with negatively charged hyaluronic acid (HA) and concurrent encapsulation of RPAB and GOx. The nanozymogen facilitated tumor accumulation via the permeability and retention (EPR) effect and the binding affinity between HA and over-expressed CD44 on cancer cell membranes. The cationic AOEI then promoted internalization of protein cargoes (RPAB and GOx) into cancer cells, and enabled endolysosomal escape via the "proton sponge" effect. The hypoxia condition along with the intracellular reductases initiated the NCs dissociation and release of GOx. GOx catalyzed the decomposition of glucose in cancer cells and simultaneously aggravated tumoral hypoxia, which not only propelled the recovery of RNase, but also expedited the degradation of AOEI to release more protein cargoes. The released GOx could further amplify the hypoxia signals and thus self-accelerate the catalytic reaction of the nanozymogen. Finally, GOx-mediated starvation therapy and RNase-mediated pro-apoptotic therapy cooperated to enable effective anti-cancer outcomes.

RPAB, the hypoxia-activatable prodrug of RNase, was synthesized via caging of the primary amines on lysine residues of RNase with azobenzene motifs. PEG-azobenzene (PAB, **compound 4**) was first synthesized via the diazotization reaction between

10.1002/anie.202004008

4-aminobenzylalcohol and phenol followed by conjugation with tosylated PEG (**compound 1**) to improve the aqueous solubility (Scheme S1, Figure S1-S4). PAB was then conjugated onto the lysine residues of RNase via a carbamate linker to yield RPAB. MALDI-TOF analysis confirmed successful conjugation of PAB onto RNase (MW = 13600 Da), and the peaks at 14998, 16194, 17537, and 18733 Da after PAB conjugation indicated that each RNase molecule was modified with 1-4 azobenzene groups (Figure 1A). After 6-h treatment with $Na_2S_2O_4$ (155 mM), the MW of RPAB recovered to that of RNase, indicating liberation of the native RNase due to hypoxia-mediated cleavage of the azobenzene linkage followed by self-immolation reaction (Scheme 1). Sodium dodecyl sulfate polyacrylamide gel electrophoresis (SDS-PAGE) analysis further demonstrated successful conjugation of PAB onto RNase, as revealed by the disappearance of the RNase band while appearance of a new band (RPAB) with increased MW (Figure 1B). When RPAB was treated with $Na_2S_2O_4$, the band of the native RNase reappeared, suggesting hypoxia-triggered liberation of the native RNase. The circular dichroism (CD) spectra of RPAB and $Na_2S_2O_4$-treated RPAB were found to be identical to that of the native RNase, indicating that the PAB caging and hypoxia-triggered PAB uncaging did not alter the secondary structure of the protein drug (Figure 1C). In support of the above findings, the hydrolytic activities of RNase and RPAB against RNA were measured using the ethidium bromide (EB) fluorescence assay (Figure 1D).[22] After addition of RNase, the fluorescence intensity was decreased due to RNase-mediated RNA degradation. In comparison, RPAB revealed minimal enzymatic activity, which however, could be completely restored after pre-treatment with $Na_2S_2O_4$. It therefore substantiated that caging of RNase with the azobenzene moiety could temporally

deactivate RNase, and hypoxia-triggered PAB cleavage could completely restore the protein function in a selective manner.

AOEI was then synthesized via chemical cross-linking of OEI (600 Da). Briefly, an azobenzene-containing cross-linker (**compound 5**) was firstly synthesized via reductive coupling of 4-nitrobenzoic acid (Scheme S2 and Figure S5), and AOEI was thereafter synthesized via the amidation reaction between **compound 5** and OEI (600 Da) (Figure S6). The MW of AOEI was determined to be 4094 Da using MALDI-TOF, and it decreased to 799 Da after 12-h treatment with $Na_2S_2O_4$ (155 mM, a reducing agent that mimics the hypoxia condition), [23] indicating the successful cross-linking of OEI and hypoxia-triggered degradation of AOEI (Figure S7). BOEI, a non-responsive analogue of AOEI with, was similarly synthesized from OEI and (1,1'-biphenyl)-4,4'-dicarboxylicacid (Scheme S2).

The inactivated RBAP and GOx were then used to construct the nanozymogen with AOEI and HA. After reaction with PAB, the negative charge density of RNase was increased due to partial caging of the cationic lysine residues (Table S1). GOx also possessed negative net charges at physiological pH. Thus, RBAP and GOx, along with the negatively charged HA, were able to form NCs with the positively charged AOEI via electrostatic interactions. Because positively charged NCs are usually toxic and unstable during circulation, it is crucial to adjust the surface charge of NCs to a negative value to minimize non-specific binding of serum proteins and enhance their biocompatibility. When the HA/AOEI weight ratio increased from 0.5 to 4, NCs with diameters of 150-200 nm could be obtained, while the zeta potential continuously decreased from +28.9 mV to -23.1 mV (Figure S8). Further enhancement of the HA/AOEI ratio did not significantly increase the negative zeta potential.

10.1002/anie.202004008

Thus, at the optimal HA/AOEI weight ratio of 4, RPAB and GOx were allowed to form the HA/AOEI/RPAB+GOx NCs (HARPG NCs, HA/AOEI/RPAB/GOx = 160/40/10/1, w/w/w/w) with the particle size of ~140 nm and negative zeta potential of -18.1 mV as determined by dynamic laser scanning (DLS) measurement (Figure 2A and Table S2). Transmission electron microscopy (TEM) observation also revealed that the HARPG NCs possessed diameter of ~120 nm with a relatively uniform size distribution (Figure 2B). The loading capacities of RPAB and GOx in the HARPG NCs were determined to be 4.4% and 0.3%, respectively. As controls, HA/AOEI/RNase NCs (HAR NCs), HA/AOEI/RPAB NCs (HARP NCs), HA/AOEI/GOx NCs (HAG NCs), and HA/AOEI/RNase+GOx NCs (HARG NCs) were similarly prepared and characterized (Table S2). After incubation with serum-containing medium for 24 h, size of the HARPG NCs remained almost constant (Figure S9), which indicated their desired serum stability due to the presence of HA that contributed to the negative surface charges. Such property would provide implications for prolonged blood circulation *in vivo*.[24]

The hypoxia-responsive dissociation of NCs was explored by TEM and DLS. As shown in Figure 2A and 2B, the NCs remarkably swelled after treatment with $Na_2S_2O_4$ for 15 min, and they partly disassembled after 4-h treatment. It thus suggested that the azobenzene groups in the cross-linked AOEI were effectively reduced under hypoxia condition, which resulted in the dissociation of NCs as a consequence of decreased molecular entanglement with protein cargoes or HA. To evaluate the hypoxia-responsive drug release profile, fluorescein isothiocyanate (FITC)-labeled RPAB and rhodamine B (RhB)-labeled GOx were synthesized and allowed to form NCs with AOEI and HA. As shown in Figure 2C, in the absence of

$Na_2S_2O_4$, only 12.2% of the total GOx was released from HARPG NCs within 24 h, suggesting the excellent GOx retention capability of HARPG NCs. In comparison, the amount of GOx released from HARPG NCs increased to 73.8% within 24 h in the $Na_2S_2O_4$-containing medium. Such a hypoxia-responsive release profile was similarly noted for RPAB, which further confirmed that hypoxia-triggered de-crosslinking of AOEI could allow "on-demand" protein release under hypoxia condition in tumor cells.

GOx could catalyze the conversion of glucose to gluconic acid, accompanied with O_2 consumption, pH decrease, and H_2O_2 production. Based on this reaction, the catalytic capability of HARPG NCs was evaluated in terms of gluconic acid and H_2O_2 production. As illustrated in Figure 2D and S10, the pH value of the glucose solution (1 mg/mL) slightly decreased from 7.0 to 6.1 after treatment with HARPG NCs for 1 h. In contrast, a drastic pH drop (from 7.0 to 3.9) occurred after incubation with $Na_2S_2O_4$-treated HARPG NCs or free GOx for 1 h, indicating the hypoxia-triggered GOx release from NCs that subsequently catalyzed glucose decomposition. In accordance, H_2O_2 concentration in the glucose solution (1 mg/mL) increased rapidly and extensively to ~2300 μmol/L after 1-h incubation with free GOx or $Na_2S_2O_4$-treated HARPG NCs (Figure 2E and S11), while the H_2O_2 concentration was only slightly increased upon incubation with HARPG NCs in the absence of $Na_2S_2O_4$ (Figure 2E). These findings demonstrated that hypoxia triggered GOx release from HARPG NCs and the released GOx preserved its enzymatic activity to decompose glucose and concomitantly consume oxygen that would potentially starve cancer cells and aggravate the hypoxia condition.

The capability of NCs to deliver protein cargoes into cancer cells was then evaluated *in*

vitro. As shown in Figure S12, after HeLa cells were incubated with HARPG NCs containing FITC-RPAB and RhB-GOx for 4 h, extensive cytoplasmic distribution of green and red fluorescence was noted, indicating the strong capability of the NCs to mediate intracellular delivery of protein cargoes. Such result was further supported by flow cytometry analysis, wherein NCs showed remarkable cellular uptake level compared to the minimal uptake level of free RPAB (Figure 3A and S13). Moreover, pre-treatment of cells with free HA significantly reduced the uptake level of HARPG NCs in HeLa cells (tumor cell) but not in 3T3 cells (fibroblast), indicating that HA facilitated cancer cell uptake of HARPG NCs by binding to the CD44 overexpressing on cancer cell surfaces. While HA mediates effective targeting of CD44 on cancer cells, it has to be admitted that CD44 is also expressed in many other cell types, which would compromise the cancer targeting selectivity of HA-based nanosystem. Anionic polymers, such as chondroitin sulfate (CS), polyglutamic acid (PGA), poly(propylacrylic acid) (PPAA), heparin, and fucosylated polysaccharide could be utilized as HA alternatives to neutralize the positive charges of NCs, and covalent conjugation with tumor-specific antibodies or aptamers may potentially enable highly effective and selective tumor targeting.

After endocytosis, NCs will experience endosomal entrapment, which prevents them from entering the cytosol. Therefore, we further evaluated the intracellular distribution of HARPG NCs containing FITC-RPAB. CLSM observation revealed extensive internalization of FITC-RPAB in HeLa cells post 4-h incubation, and the green fluorescence of FITC-RPAB largely separated from the red fluorescence of Lysotracker Red-stained endosomes (Figure S14), suggesting that the HARPG NCs were capable of mediating effective endosomal escape,

presumably due to the AOEI-assisted proton sponge mechanism.[25]

Then, hypoxia-triggered intracellular protein release, GOx-mediated H_2O_2 generation, and HARPG NCs-aggravated hypoxia in tumor cells were investigated. A hypoxia/oxidative stress (ROS) detection kit was first used to detect the intracellular H_2O_2 generation and the concomitant aggravation of local hypoxia after incubation of HeLa cells with HARPG NCs. As shown in Figure 3B, free GOx induced a slightly higher level of intracellular hypoxia than deferoxamine (DFO), a hypoxia inducer, as indicated by the intensified magenta fluorescence generated by the hypoxia probe. Cells treated with HARPG NCs showed the strongest magenta fluorescence intensity, indicating the capabilities of NCs to facilitate intracellular GOx delivery that catalyzed the decomposition of glucose accompanied with oxygen consumption. Cells treated with HARPG NCs also showed the strongest green fluorescence of the ROS probe, which consistently demonstrated the generation of intracellular H_2O_2 as a product of glucose decomposition (Figure S15). Such finding was further supported by the quantitative analysis using flow cytometry, wherein cells treated with HARPG NCs showed remarkably higher levels of cellular hypoxia (48.6%) and ROS (46.1%) levels than GOx-treated and un-treated cells (Figure 3C).

To further investigate the hypoxia-triggered intracellular protein release, HARP NCs consisting of rhodamine-labeled AOEI (RhB-AOEI) and FITC-labeled RPAB (FITC-RPAB) were incubated with HeLa cells for 4 h and the colocalization between the fluorescence of RhB-AOEI and FITC-RPAB was calculated. As shown in Figure 3D and 3E, notable fluorescence separation was noted under hypoxia concentrations (5% and 1% O_2) compared to the fluorescence overlap under normoxia (20% O_2), conferring decreased colocalization

ratios of 81.1%, 64.0%, and 41.1% at the oxygen levels of 20%, 5%, and 1%, respectively. Similar fluorescence separation was also noted for cells treated with HARPG NCs containing RhB-AOEI and FITC-RPAB under norxomia condition (Figure S16). In contrast, unappreciable fluorescence separation was noted for HA/BOEI/RPAB (HBRP) NCs containing the non-responsive RhB-BOEI and FITC-RPAB either under hypoxia or normoxia conditions (Figure S17). These results thus collectively substantiated that sufficient hypoxia could lead to protein release as a consequence of AOEI degradation, and HARPG NCs could enhance oxygen consumption upon initial GOx release induced by mild hypoxia, which enabled cyclic amplification of the hypoxia trigger signals and thus self-catalyzed the protein release.

Polycatioic materials tend to cause cell damage, because of their strong interactions with cell membranes. Thus, prior to the *in vitro* anti-cancer efficacy study, the cytotoxicity of AOEI was first monitored in HeLa cells under both normoxia (20% O_2) and hypoxia (1% O_2) environmenets. AOEI displayed concentration-dependent cytotoxicity under normoxia condition, while it showed negligible cytotoxicity under hypoxia at the concentration up to 35 μg/mL (Figure 4A), indicating that hypoxia-triggered degradation of AOEI into low-MW segments to diminish the materials toxicity. As a control, the non-responsive BOEI revealed similar cytotoxicity under both normoxia and hypoxia conditions (Figure S18), which further confirmed that hypoxia-triggered polymer degradation could greatly reduced the materials toxicity.

Then, the *in vitro* anti-cancer efficacy of various NCs in HeLa cells was evaluated using the MTT assay. As shown in Figure 4B and Figure 4C, HARP NCs showed minimal

10.1002/anie.202004008

cytotoxicity under normoxia at the RPAB concentration up to 2 μg/mL, indicating deprivation of the catalytic activity of the protein drug. However, HARP NCs showed concentration-dependent cytotoxicity under hypoxia (1% O_2), which was similar to that of HAR NCs under either hypoxia or normoxia conditions (Figure 4C and 4D), substantiating hypoxia-mediated recovery of the prodrug RPAB to the catalytically active RNase. HAG NCs also exhibited a concentration-dependent anticancer activity in presence of O_2 (Figure 4B), which was ascribed to the consumption of glucose that starved the tumor cells and generation of intracellular H_2O_2 that caused apoptosis of tumor cells. Because O_2 was continuously consumed during GOx-mediated starvation therapy, it created a more hypoxic environment that would facilitate the dissociation of NCs to release more GOx, thus realizing the cyclic amplication of hypoxia signals. In accompany with such enzyme-linked reaction, more RPAB could also be released from HARPG NCs and be recovered to RNase upon hypoxia. In support of such mechanism, the anti-cancer efficacy of HARPG NCs was significantly stronger than HAG NCs and similar to that of HARG NCs (Figure 4B), indicating GOx-assisted recovery of the prodrug RPAB back to RNase which subsequently provoked cooperative anti-cancer effect with GOx. Similar trend was noted when the cancer cell apoptosis level was determined using the Annexin V-fluoresceine isothiocyanate (Annexin V-FITC)/propidine iodide (PI) apoptosis detection assay. As shown in Figure 4E, HARP NCs induced minimal cancer cell apoptosis, while HARPG NCs and HARG NCs provoked similar and the highest apoptosis levels of 50.7% and 56.2%, notably outperforming the HAR NCs (19.4%) and HAG NCs (31.6%). When AOEI was replaced by the non-degradable BOEI, the anti-cancer efficacies of NCs were significantly decreased (Figure S19), which further

evidenced that the hypoxia-responsive AOEI degradation was critical to the cytosolic release and bioactivity of protein cargoes.

The pharmacokinetics and biodistribution of HARPG NCs after i.v. injection were then explored. As shown in Figure 5A, the blood circulation half-life ($t_{1/2}$) of HARPG NCs containing Cy5-RPAB (~4.16 h) was about 8-fold longer than that of free Cy5-RPAB (~0.51 h), mainly because HA shielded the positive surface charges of NCs and sterically hindered the binding of blood components. The biodistribution of Cy5-RPAB-containing HARPG NCs and free Cy5-RPAB was then evaluated in HeLa xenograft tumor-bearing mice using the live animal imaging system. As shown in Figure 5B, the fluorescence of HARPG NCs at the tumor site steadily increased and peak at 24 h post i.v. injection, while in comparison, negligible fluorescence was observed in tumors administered with Cy5-RPAB. Thus, tumors and major organs were harvested at 24 h post injection and subjected to *ex vivo* imaging. The fluorescence intensity in NCs-treated tumors was 4.1-fold of that in free Cy5-RPAB-treated tumors, which could be attributed to the prolonged circulation and HA-mediated tumor targeting capability of NCs (Figure 5C and 5D).

To investigate whether the HARPG NCs could exacerbate hypoxia in the solid tumors, *in vivo* photoacoustic (PA) imaging was adopted to monitor the blood oxygenation status (sO_2) in tumors via detection of oxyhemoglobin saturation. As shown in Figure 5E and 5F, the sO_2 level in tumors dramatically decreased from 46.6% at 0 h to 14.1% at 24 h post i.v. injection of HARPG NCs. In comparison, no obvious change of tumoral sO_2 level was observed in mice injected with HARP NCs deprived of GOx. Free GOx, after i.v. injection, led to slight decrease of the tumoral sO_2 level, mainly due to the low tumor accumulation level and fast

clearance. These findings therefore evidenced that HARPG NCs could lead to aggravation of hypoxia in the tumor tissues in accompany with GOx-mediated glucose decomposition, which could subsequently accelerate the hypoxia-instructed NCs dissociation, protein cargo release, and activation of RPAB.

The *in vivo* anti-tumor efficacy of the nanozymogen was evaluated in HeLa xenograft tumor-bearing mice following i.v. injection. As shown in Figure 6A and 6B, no significant tumor inhibition was observed for HARP NCs, because RPAB was deprived of the enzymatic activity after caging of RNase with azobenzene motifs. HAR NCs capable of RNase-mediated tumor inhibition and HAG NCs capable of GOx-mediated tumor starvation showed moderate anti-cancer efficacies, conferring the tumor growth inhibition (TGI) rates of 75.5% and 77.2%, respectively. Comparatively, HAPRG NCs led to notably higher tumor remission, representing the TGI rate of 97.6% that was similar to that of HARG NCs. In accordance, HARPG NCs led to the highest animal survival rate within the 45-d observation period (Figure 5C), and they induced the highest levels of tumor cell apoptosis and remissioin (Figure 5D and S21). These findings thus substantiated the re-activation of RPAB in tumors in response to GOx-aggravated hypoxia, which concomitantly provoked cooperative anti-cancer outcomes. The body weights of mice were not significantly affected within the 19-d observation period upon administrations of various NCs (Figure S20), implying lack of appreciable systemic toxicity of NCs.

The *in vivo* biocompatibility of NCs was finally evaluated in terms of hematological analysis, blood biochemical measurement, and histological observation. On day 1, 3, and 5, PBS or various NCs were i.v. injected using the same protocol as in the efficacy study, and

biocompatibility evaluation was performed at 24 h post the third injection. Lack of abnormality was noted for all hematological and biochemical parameters after administration of various NCs (Figure S22). In the homogenate of liver, spleen, and kidney, alanine aminotransferase (ALT), aspartate aminotransferase (AST), alkaline phosphatase (ALP), lipid peroxidation (LPO), and creatinine (CR) levels showed no significant change after treatment with various NCs (Figure S23). Additionally, the levels of pro-inflammatory cytokines (TNF-α, IL-6, and IL-1β) in these organs did not significantly change after administration of NCs (Figure S23). HE staining of major organs also revealed lack of pathological indications (Figure S24). These results therefore collectively indicated that the NCs did not cause appreciable systemic toxicity or inflammatory response.

In summary, were herein reported a cascaded anti-cancer nanozymogen that incorporated hypoxia-instructed pro-protein engineering and hypoxia-strengthened intracellular protein delivery to enable potent anti-cancer protein therapy. RPAB, a hypoxia-activatable pro-protein of RNase, was designed and co-delivered with GOx using a hypoxia-dissociable nanosystem to enable efficient intracellular protein therapy in cancer cells. To the best of our knowledge, this study represents the first example of hypoxia-responsive pro-protein engineering, and when coupled with the GOx-mediated, self-catalyzed hypoxia aggravation mechanism, it provides highly sensitive and selective control over the protein activities in tumor cells. We thus believe that the current approach expands the available chemical tools for the conditional and precision control over the structure and function of proteins. In addition, such a hypoxia-dissociable nanosystem that is capable of GOx-strengthened, hypoxia-assisted intracellular protein release also provides innovative insights into the design

of intracellular protein delivery vehicles.

Acknowledgment

This work was supported by the Ministry of Science and Technology of China (2016YFA0201200), the National Natural Science Foundation of China (51722305 and 51873142), 111 project, and Priority Academic Program Development of Jiangsu Higher Education Institutions (PAPD).

References

[1] B. Leader, Q. J. Baca, D. E. Golan, *Nat. Rev. Durg Discov.* **2008**, *7*, 21-39.

[2] a) S. Marchal, A. El Hor, M. Millard, V. Gillon, L. Bezdetnaya, *Drugs* **2015**, *75*, 1601-1611; b) J. Shi, P. W. Kantoff, R. Wooster, O. C. Farokhzad, *Nat. Rev. Cancer* **2017**, *17*, 20-37.

[3] L. Urquhart, *Nat. Rev. Durg Discov.* **2018**, *17*, 309-309.

[4] A. N. Zelikin, C. Ehrhardt, A. M. Healy, *Nat. Chem.* **2016**, *8*, 997-1007.

[5] a) P. J. Carter, *Nat. Rev. Immunol.* **2006**, *6*, 343-357; b) J. Lv, Q. Fan, H. Wang, Y. Cheng, *Biomaterials* **2019**, *218*, 119358; c) S. Mitragotri, P. A. Burke, R. Langer, *Nat. Rev. Durg Discov.* **2014**, *13*, 655-672.

[6] a) C. Liu, T. Wan, H. Wang, S. Zhang, Y. Ping, Y. Cheng, *Sci. Adv.* **2019**, *5*, eaaw8922; b) Z. Zhang, W. Shen, J. Ling, Y. Yan, J. Hu, Y. Cheng, *Nat. Commun.* **2018**, *9*, 1-8; c) L. Ren, J. Lv, H. Wang, Y. Cheng, *Angew. Chem. Int. Ed.* **2019**, *132*, 4741-4749.

[7] a) K. Dutta, D. Hu, B. Zhao, A. E. Ribbe, J. Zhuang, S. Thayumanavan, *J. Am. Chem. Soc.* **2017**, *139*, 5676-5679; b) J. Ren, Y. Zhang, J. Zhang, H. Gao, G. Liu, R. Ma, Y. An, D. Kong, L. Shi, *Biomacromolecules* **2013**, *14*, 3434-3443.

[8] a) M. Yan, J. Du, Z. Gu, M. Liang, Y. Hu, W. Zhang, S. Priceman, L. Wu, Z. H. Zhou, Z. Liu, *Nat. Nanotechnol.* **2010**, *5*, 48-53; b) M. Zhao, Y. Liu, R. S. Hsieh, N. Wang, W. Tai, K.-I. Joo, P. Wang, Z. Gu, Y. Tang, *J. Am. Chem. Soc.* **2014**, *136*, 15319-15325; c) D. Wu, M. Qin, D. Xu, L. Wang, C. Liu, J. Ren, G. Zhou, C. Chen, F. Yang, Y. Li, *Adv. Mater.* **2019**, *31*, 1807557.

[9] M. Wang, J. A. Zuris, F. Meng, H. Rees, S. Sun, P. Deng, Y. Han, X. Gao, D. Pouli, Q. Wu, *Proc. Natl. Acad. Sci. USA* **2016**, *113*, 2868-2873.

[10] a) M. Liu, S. Shen, D. Wen, M. Li, T. Li, X. Chen, Z. Gu, R. Mo, *Nano Lett.* **2018**, *18*, 2294-2303; b) J. R. Clegg, A. S. Irani, E. W. Ander, C. M. Ludolph, A. K. Venkataraman, J. X. Zhong, N. A. Peppas, *Sci. Adv.* **2019**, *5*, eaax7946; c) S. Su, Y. Y. Wang, F. S. Du, H. Lu, Z. C. Li, *Adv. Funct. Mater.* **2018**, *28*, 1805287.

[11] a) T.-T. Chen, J.-T. Yi, Y.-Y. Zhao, X. Chu, *J. Am. Chem. Soc.* **2018**, *140*, 9912-9920; b) P. Yuan, H. Zhang, L. Qian, X. Mao, S. Du, C. Yu, B. Peng, S. Q. Yao, *Angew. Chem. Int. Ed.* **2017**, *56*, 12481-12485; c) P. Yuan, X. Mao, X. Wu, S. S. Liew, L. Li, S. Q. Yao, *Angew. Chem. Int. Ed.* **2019**, *131*, 7739-7743; d) D. Shao, M. Li, Z. Wang, X. Zheng, Y. H. Lao, Z. Chang, F. Zhang, M. Lu, J. Yue, H. Hu, H. Yan, L. Chen, W. F. Dong, K. W.

Leong, *Adv. Mater.* **2018**, *30*, 1801198.

[12] a) D. Y. Ng, M. Arzt, Y. Wu, S. L. Kuan, M. Lamla, T. Weil, *Angew. Chem. Int. Ed.* **2014**, *53*, 324-328; b) Y. Ma, Y. Zhao, N. K. Bejjanki, X. Tang, W. Jiang, J. Dou, M. I. Khan, Q. Wang, J. Xia, H. Liu, *ACS Nano* **2019**, *13*, 8890-8902; c) L. Zhang, Z. Wang, Y. Zhang, F. Cao, K. Dong, J. Ren, X. Qu, *ACS Nano* **2018**, *12*, 10201-10211; d) D. Yuan, Y. Zhao, W. A. Banks, K. M. Bullock, M. Haney, E. Batrakova, A. V. Kabanov, *Biomaterials* **2017**, *142*, 1-12.

[13] F. Wu, T. Jin, *Aaps Pharmscitech* **2008**, *9*, 1218-1229.

[14] a) Q.-Y. Hu, F. Berti, R. Adamo, *Chem. Soc. Rev.* **2016**, *45*, 1691-1719; b) M. R. Battig, B. Soontornworajit, Y. Wang, *J. Am. Chem. Soc.* **2012**, *134*, 12410-12413.

[15] P. Mahlumba, Y. E. Choonara, P. Kumar, L. C. Du Toit, V. Pillay, *Molecules* **2016**, *21*, 1002-1002.

[16] a) X. Liu, P. Zhang, D. He, W. Rödl, T. Preiß, J. O. Rädler, E. Wagner, U. Lächelt, *Biomacromolecules* **2016**, *17*, 173-182; b) A. Kim, Y. Miura, T. Ishii, O. F. Mutaf, N. Nishiyama, H. Cabral, K. Kataoka, *Biomacromolecules* **2016**, *17*, 446-453; c) M. Wang, K. Alberti, S. Sun, C. L. Arellano, Q. Xu, *Angew. Chem. Int. Ed.* **2014**, *53*, 2893-2898.

[17] a) M. Wang, S. Sun, C. I. Neufeld, B. Perez‐Ramirez, Q. Xu, *Angew. Chem. Int. Ed.* **2014**, *53*, 13444-13448; b) B. Liu, M. Ianosi-Irimie, S. Thayumanavan, *ACS Nano* **2019**, *13*, 9408-9420; c) T. T. Hoang, T. P. Smith, R. T. Raines, *Angew. Chem. Int. Ed.* **2017**, *56*, 2619-2622.

[18] J. Chang, W. Cai, C. Liang, Q. Tang, X. Chen, Y. Jiang, L. Mao, M. Wang, *J. Am. Chem. Soc.* **2019**, *141*, 18136-18141.

[19] a) H. He, Y. Chen, Y. Li, Z. Song, Y. Zhong, R. Zhu, J. Cheng, L. Yin, *Adv. Funct. Mater.* **2018**, *28*, 1706710; b) J. Li, C. Xie, J. Huang, Y. Jiang, Q. Miao, K. Pu, *Angew. Chem. Int. Ed.* **2018**, *57*, 3995-3998.

[20] D. Huo, X. Jiang, Y. Hu, *Adv. Mater.* **2019**, 1904337, doi:1904310.1901002/adma.201904337.

[21] a) L. H. Fu, C. Qi, Y. R. Hu, J. Lin, P. Huang, *Adv. Mater.* **2019**, *31*, 1808325; b) S. B. Bankar, M. V. Bule, R. S. Singhal, L. Ananthanarayan, *Biotechnol. Adv.* **2009**, *27*, 489-501.

[22] X. Liu, P. Zhang, D. He, W. Rödl, T. Preiß, J. O. Rädler, E. Wagner, U. Lächelt, *Biomacromolecules* **2015**, *17*, 173-182.

[23] S. H. Lee, E. Moroz, B. Castagner, J.-C. Leroux, *J. Am. Chem. Soc.* **2014**, *136*, 12868-12871.

[24] K. Y. Choi, H. S. Han, E. S. Lee, J. M. Shin, B. D. Almquist, D. S. Lee, J. H. Park, *Adv. Mater.* **2019**, *31*, 1803549.

[25] R. V. Benjaminsen, M. A. Mattebjerg, J. R. Henriksen, S. M. Moghimi, T. L. Andresen, *Mol. Ther.* **2013**, *21*, 149-157.

10.1002/anie.202004008

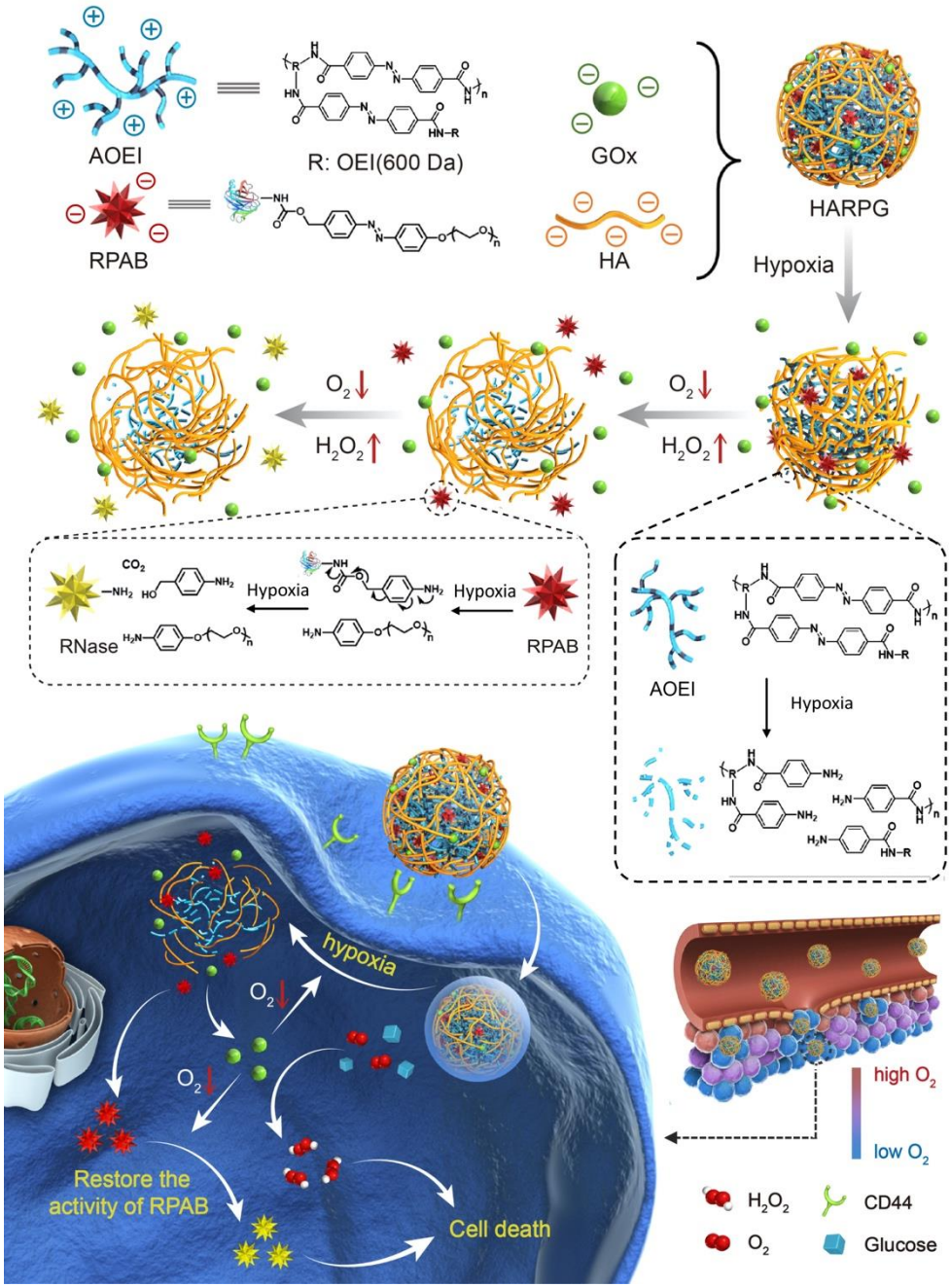

Scheme 1. Schematic illustration of cascaded, self-catalyzed nanozymogen incorporating hypoxia-instructed pro-protein engineering and hypoxia-strengthened intracellular protein delivery. RPAB, a pro-protein of RNase A reversibly caged with hypoxia-cleavable azobenzene, was designed and co-delivered with GOx using hypoxia-dissociable NCs consisting of AOEI and HA. Upon systemic injection, the nanozymogen mediated efficient tumor accumulation, targeted internation in cancer cells, and effective endolysosomal escape. GOx catalyzed intracellular glucose decomposition and aggravated tumoral hypoxia, which drove the recovery of RPAB back to the hydrolytically active RNase and concurrently expedited the degradation of AOEI to release more protein cargoes. Thus, the catalytic reaction of the nanozymogen was self-accelerated and self-cycled, ultimately leading to

10.1002/anie.202004008

cooperative anti-cancer efficacies between GOx-mediated starvation therapy and RNase-mediated pro-apoptotic therapy.

10.1002/anie.202004008

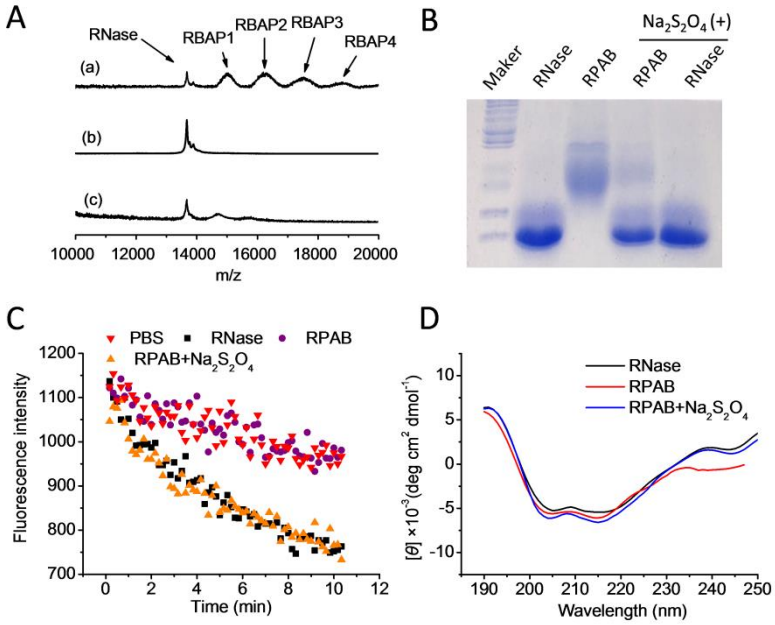

Figure 1. Characterization and hypoxia-triggered re-activation of RPAB. A) MALDI-TOF spectra of (a) RPAB, (b) RNase, and (c) RPAB treated with $Na_2S_2O_4$ (155 mM). B) SDS-PAGE of RNase and RPAB with or without $Na_2S_2O_4$ treatment (155 mM). C) Enzymatic activity of RNase, RPAB, and $Na_2S_2O_4$ (155 mM)-treated RPAB as measured by the EB assay (n = 3). D) CD spectra of RNase, RPAB, and $Na_2S_2O_4$ (155 mM)-treated RPAB.

10.1002/anie.202004008

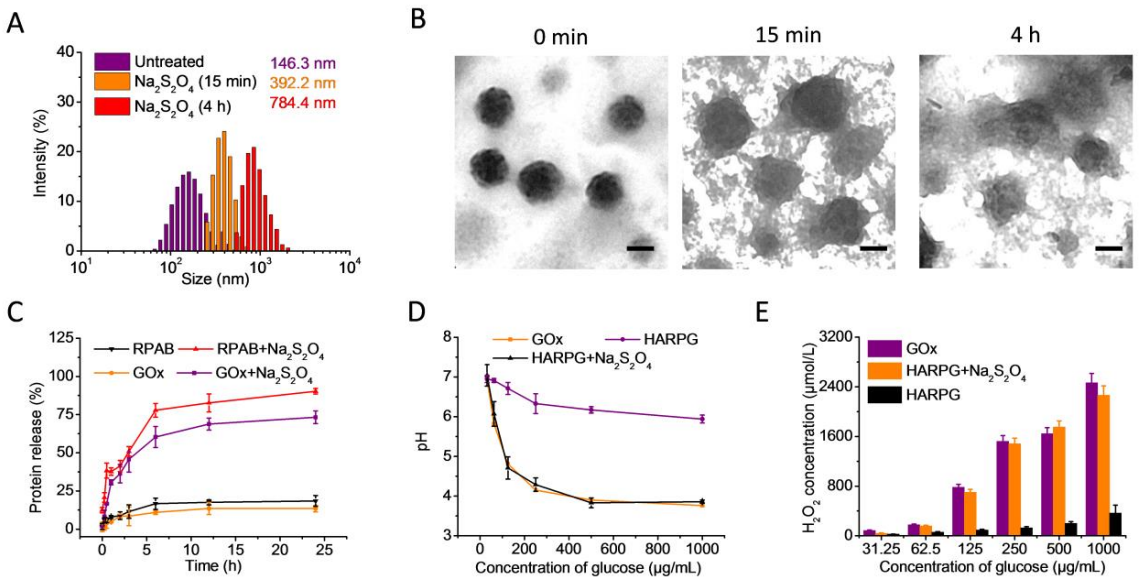

Figure 2. Hypoxia-triggered protein release from NCs and GOx-mediated glucose decomposition. Size A) and TEM images B) of HARPG NCs before and after $Na_2S_2O_4$ treatment (155 mM) for different time. Scale bar = 100 nm. C) RPAB and GOx release from HARPG in PBS (pH 7.4) with or without $Na_2S_2O_4$ (155 mM) (n = 3). D) pH values of glucose solutions at different concentrations after 1-h incubation with free GOx, HARPG NCs, and $Na_2S_2O_4$ (155 mM)-treated HARPG NCs (n = 3). E) H_2O_2 concentrations of glucose solutions at different concentrations after 1-h incubation with free GOx, HARPG NCs, and $Na_2S_2O_4$ (155 mM)-treated HARPG NCs (n = 3).

10.1002/anie.202004008

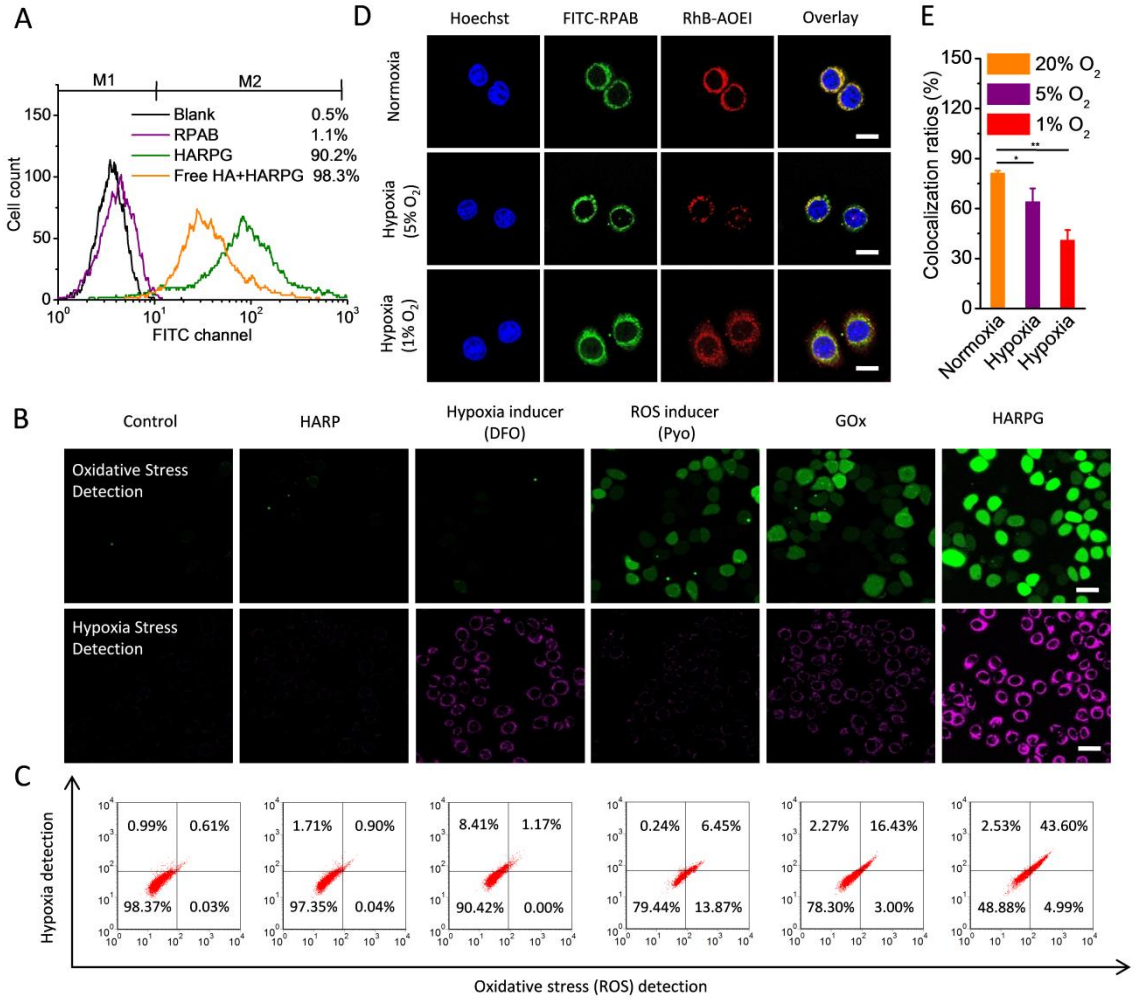

Figure 3. Cancer cell-targeted intracellular protein delivery, hypoxia-triggered intracellular protein release, and aggravation of intracellular hypoxia mediated by HARPG NCs *in vitro*. A) Uptake of HARPG NCs containing FITC-RPAB in HeLa cells following 4-h incubation as evaluated by flow cytometry. HeLa cells were pre-treated with HA for 4 h to block CD44 and the HA-mediated targeting effect. B) CLSM images of HeLa cells treated with free GOx, HARP NCs, and HARPG NCs for 4 h followed by staining with hypoxia/ROS detection probes. DFO and Pyo served as positive controls for ROS and hypoxia induction, respectively. Scale bar = 50 μm. C) Flow cytometry analysis of intracellular ROS and hypoxia levels following the same treatment in B) (n = 3). D) CLSM images of HeLa cells following incubation with HARP NCs containing FITB-RPAB and RhB-AOEI under hypoxia or normoxia at 37 ^{o}C for 4 h. Cell nuclei were stained with DAPI. Scale Bar = 15 μm. E) Colocalization ratios between the fluorescence of FITC-RPAB and RhB-AOEI as calculated from CLSM images in D) (n = 20).

10.1002/anie.202004008

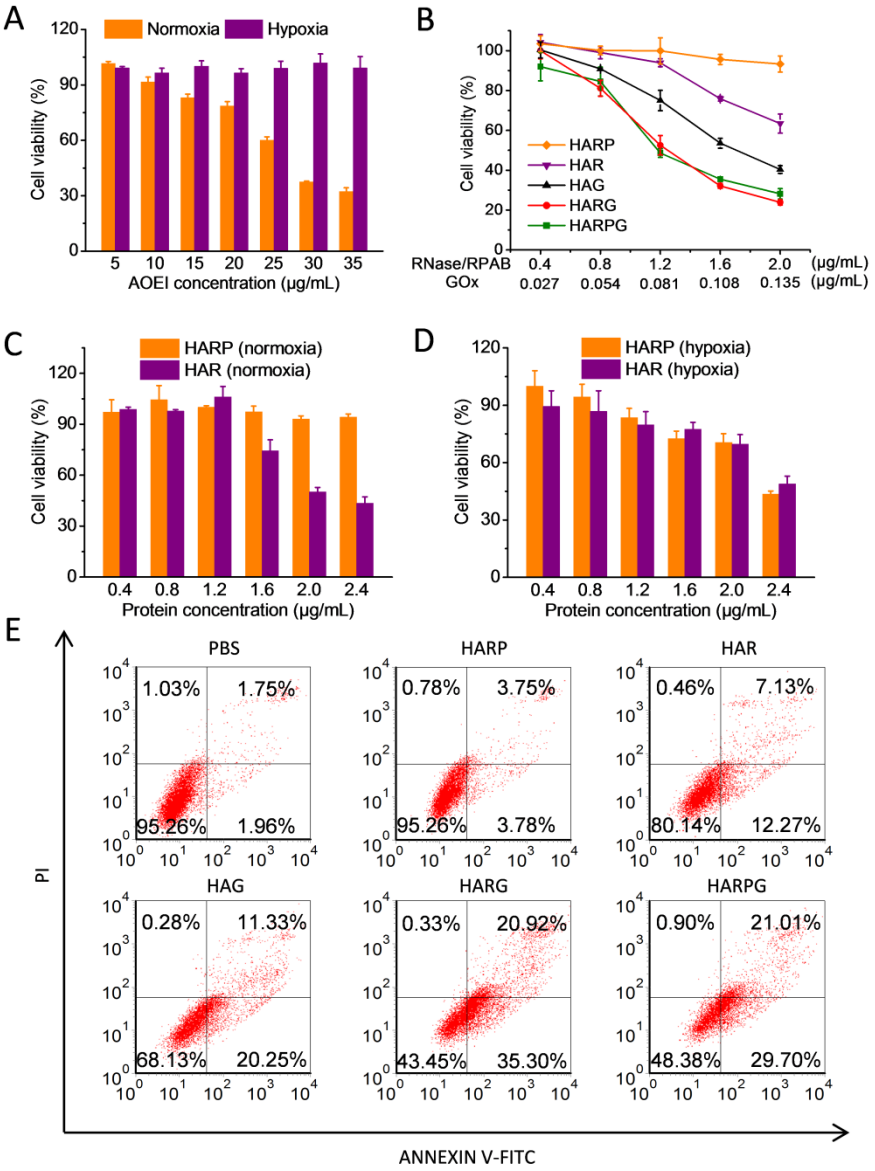

Figure 4. Anti-cancer efficacy of HARPG NCs in HeLa cells *in vitro*. A) Cytotoxicity of HA/AOEI NCs (w/w = 4/1) following 48-h incubation under normoxia or hypoxia at various AOEI concentrations (n = 3). B) Cytotoxicity of different NCs after 48-h incubation under normoxia (n = 3). Cytotoxicity of HARP NCs and HAR NCs after 48-h incubation under normoxia C) or hypoxia D) at various RNase/RPAB concentrations (n = 3). (E) Flow cytometric analysis of HeLa cells treated with different NCs for 48 h and stained with Annexin V-FITC/PI.

10.1002/anie.202004008

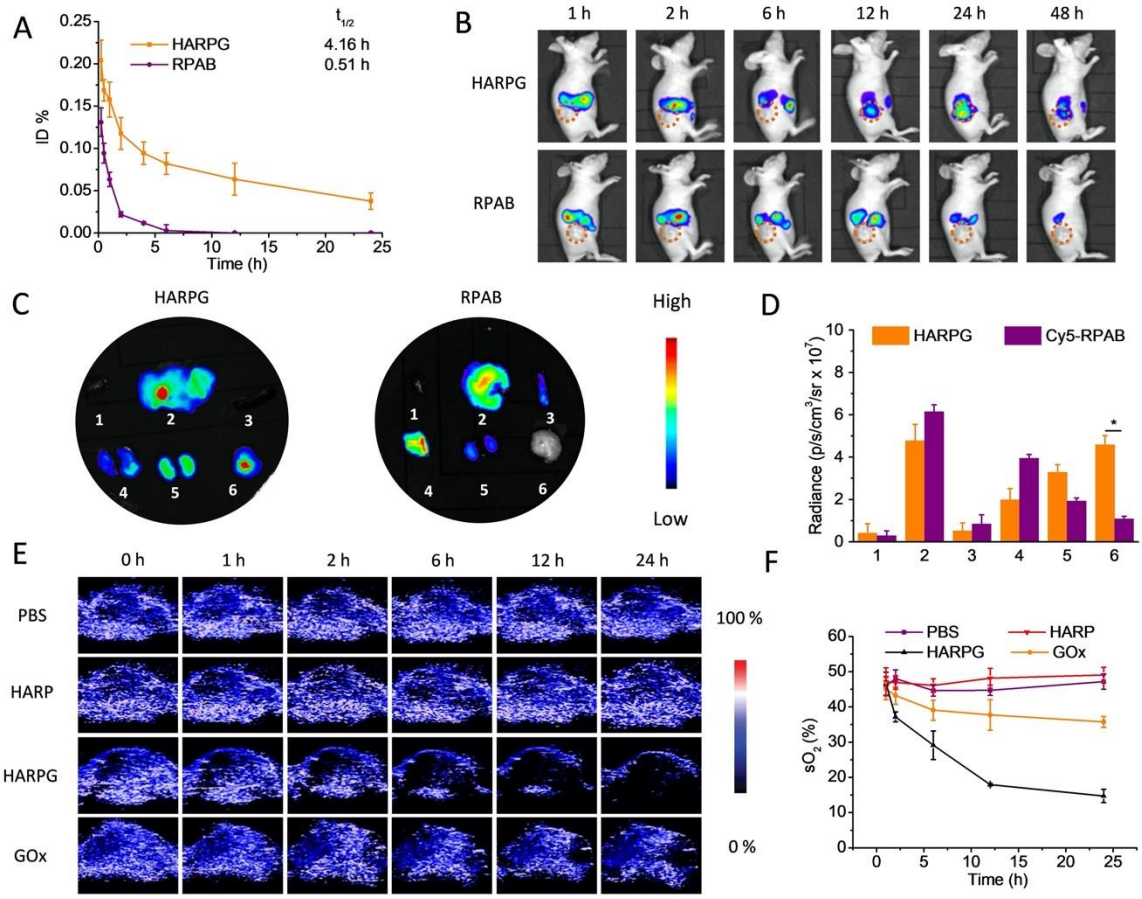

Figure 5. Pharmacokinetics and biodistribution HARPG NCs and their capabilities to aggravate hypoxia in tumors *in vivo*. A) Pharmacokinetics of Cy5-RPAB-containing HARPG NCs and free Cy5-RPAB in mice following i.v. injection at 2.5 mg/kg RPAB (n = 3). B) Fluorescence imaging of HeLa tumor-bearing mice at different time points post i.v. injection of Cy5-RPAB-containing HARPG NCs and free Cy5-RPAB (2.5 mg/kg RPAB). The red circle indicates the tumor site. C) *Ex vivo* fluorescence imaging of excised tumors and major organs at 24 h post i.v. injection (1: heart; 2: liver; 3: spleen; 4: lung; 5: kidney; 6: tumor). D) Calculated fluorescence intensity of each tissue in (C) (n = 3). E) PA imaging of tumors by measuring deoxygenated hemoglobin and oxygenated hemoglobin at different time points post i.v. injection of PBS, HARP NCs, HARPB NCs, or free GOx (1 mg/kg GOx). (F) Calculated oxyhemoglobin saturation levels in tumors from PA imaging in (D) (n = 3).

10.1002/anie.202004008

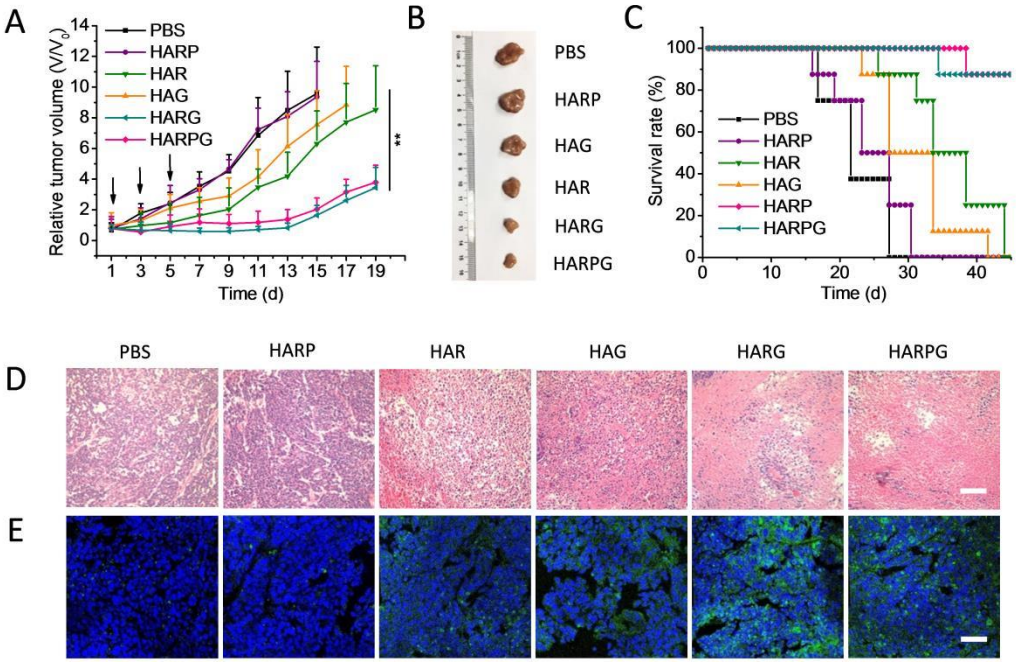

Figure 6. *In vivo* cooperative anti-tumor efficacy of HARPG NCs against HeLa xenograft tumors. PBS, HARP NCs, HAR NPs, HAG NCs, HARG NCs, and HARPG NCs were i.v. injected on day 1, 3, and 5 (RPAB, 2.5 mg/kg; RNase, 2.5 mg/kg; GOx, 1 mg/kg). (A) Tumor volume progression within the 19-d observation period (n = 11). Arrows represent the injection time. (B) Representative images of tumors harvested on day 19. (C) Survival rate of mice within the 45-d observation period (n = 8). (D) H&E-stained tumor tissues harvested on day 6. Scale bar = 100 μm. (E) Cell apoptosis in tumor tissues harvested on day 6 as determined by TUNEL staining. Scale bar = 100 μm.

10.1002/anie.202004008

TOC image

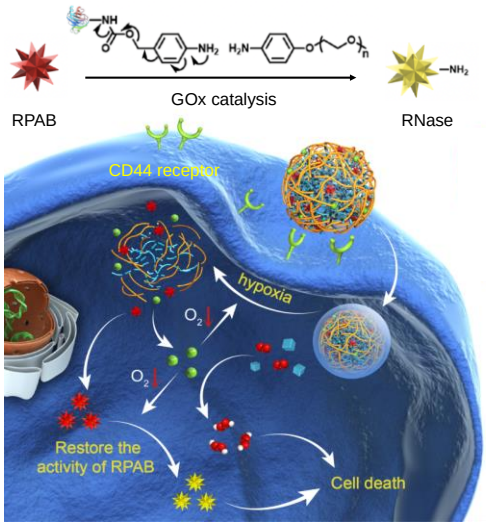

Cascaded nanozymogen was designed to incorporate hypoxia-instructed pro-protein engineering and hypoxia-strengthened intracellular protein delivery. Hypoxia-activatable pro-protein and GOx were encapsulated within cell-ingestable and hypoxia-dissociable NCs. Upon GOx-catalyzed hypoxia aggravation, cascaded intracellular reactions of pro-protein reactivation, NCs dissociation, and protein release were self-catalyzed and self-cycled, thus provoking efficient and selective anti-cancer efficacies.